ARMY RESEARCH LABORATORY

Mechanical Performance of Austempered Ductile Iron

David K. Matlock and George Krauss

ARL-CR-117 April 1994

Prepared by

Advanced Steel Processing and
Products Research Center
Department of Metallurgical and Materials Engineering
Colorado School of Mines, Golden, CO 80401

under contract

EEC9147146
(National Science Foundation)

The findings in this report are not to be construed as an official Department of the Army position unless so designated by other authorized documents.

Citation of manufacturer's or trade names does not constitute an official endorsement or approval of the use thereof.

Destroy this report when it is no longer needed. Do not return it to the originator.

REPORT DOCUMENTATION PAGE

Form Approved
OMB No. 0704-0188

1. AGENCY USE ONLY (Leave blank)	2. REPORT DATE	3. REPORT TYPE AND DATES COVERED
	April 1994	Final Report - 2/93 - 12/93

4. TITLE AND SUBTITLE
Mechanical Performance of Austempered Ductile Iron

5. FUNDING NUMBERS
Contract No. EEC9147146 (National Science Foundation)

6. AUTHOR(S)
David K. Matlock and George Krauss

7. PERFORMING ORGANIZATION NAME(S) AND ADDRESS(ES)
Advanced Steel Processing and Products Research Center
Dept. of Metallurgical and Materials Engineering
Colorado School of Mines, Golden, CO 80401

8. PERFORMING ORGANIZATION REPORT NUMBER

9. SPONSORING/MONITORING AGENCY NAME(S) AND ADDRESS(ES)
U.S. Army Research Laboratory
Watertown, MA
ATTN: AMSRL-OP-PR-WT

10. SPONSORING/MONITORING AGENCY REPORT NUMBER
ARL-CR-117

11. SUPPLEMENTARY NOTES
Martin G. H. Wells COR

12a. DISTRIBUTION/AVAILABILITY STATEMENT
Approved for public release, distribution unlimited.

12b. DISTRIBUTION CODE

13. ABSTRACT (Maximum 200 words)

Plates of Austempered Ductile Iron (ADI) containing, in mass pct, 3.7 C, 2.7 Si, 0.97 Ni and 0.27 Mn were heat treated to ASTM 897 Grade 1 and 3 tensile properties and subjected to tensile testing at temperatures between -80 and 120 °C. Room temperature yield and ultimate tensile strengths met specifications but values of elongation were lower than expected. The retained austenite contents contributed to lowered yield strengths during low temperature testing and increased ultimate tensile strengths and ductilities during high temperature testing. These changes in properties were related to the effects of temperature on the strain-induced transformation of austenite to martensite. The lower than expected ductility of the ADI specimens was related to microporosity, differences in graphite nodule distributions, differences in strain hardening related to austenite stability, and the ductile-to-brittle fracture transition of the matrix ferrite with decreasing temperature.

14. SUBJECT TERMS	15. NUMBER OF PAGES
Ductile iron, Austempering, Mechanical properties, Austenite transformation	35
	16. PRICE CODE

17. SECURITY CLASSIFICATION OF REPORT	18. SECURITY CLASSIFICATION OF THIS PAGE	19. SECURITY CLASSIFICATION OF ABSTRACT	20. LIMITATION OF ABSTRACT
Unclassified	Unclassified	Unclassified	UL

1.0 INTRODUCTION

Austempered ductile irons (ADI) are alloyed nodular cast irons which after solidification are subjected to austenitizing and isothermal transformation (austempering) heat treatments (1,2). During isothermal holding, austenite first transforms to acicular or bainitic ferrite and carbon is rejected into austenite adjacent to the ferrite. The high silicon of the cast iron prevents cementite formation, and the enriched austenite, sometimes referred to as reacted austenite (3), is quite stable and coexists with the acicular ferrite to provide good combinations of strength and ductility (4). Adjustments in austenitizing and austempering temperatures are used to produce ADI grades of various strength and ductility levels (5). The grade designations, minimums in strength and ductility, and anticipated hardness ranges are summarized in Table 1. These data show that depending on heat treatment, tensile strengths between 125 ksi and 220 ksi can be obtained. Extended heating in the austempering range could cause the retained austenite to decompose to ferrite-carbide microstructures with reduced toughness (5).

TABLE 1 - Summary of Tensile Properties for Standard ADI Grades as Specified in ASTM 897-90 (5).

Grade	Tensile Strength* (ksi)	Yield Strength* (ksi)	Elongation* (%)	Typical Hardness (BHN)
1	125	80	10	269-321
2	150	100	7	302-363
3	175	125	4	341-444
4	200	155	1	388-477
5	230	185	N/A	444-555

* Minimum Values

Recent studies of intercritically annealed and isothermally transformed low-carbon steels show that retained austenite plays an important role in mechanical behavior (6-9). Depending on test temperature, the austenite may transform at low strains and significantly affect yielding behavior, or the austenite may be stable to high strains and enhance ultimate strength and defer necking instability.

The effect of test temperature on the mechanical behavior of the ferrite-austenite-nodular graphite microstructures of ADI has received relatively little attention. Therefore, the purpose of this investigation was to evaluate mechanical performance of ADI by tensile testing over a range of temperatures, from cryogenic to well above room temperature. The selected range of temperatures represents conditions to which ADI tank components might be subjected in climates ranging from desert to arctic.

2.0 EXPERIMENTAL PROCEDURE

The research program involved three specific phases identified as follows:

Phase I	Microstructural and hardness analysis of as-cast plates and laboratory heat treated coupons.
Phase II	Mechanical property study on laboratory heat treated samples.
Phase III	Mechanical property study on commercially heat treated Grade 1 and Grade 3 samples.

Experimental castings were prepared by Wagner Casting Company, Decator, Illinois, as either 0.5 inch (12.7mm) or 1.0 inch (25.4 mm) thick plates with the following composition (in wt. pct.): 3.7 C, 2.7 Si, 0.97 Ni, 0.27 Mn, 0.057 Mg, 0.003 Mo, 0.87 Cu, 0.009 P, 0.009 S, and 0.03 Cr. Two 8 x 8 inch plates of each thickness were received in the as-cast condition for Phase I and Phase II studies. The material for Phase III was received in commercially heat treated conditions.

2.1 Phase I

The as-received microstructures of each thickness plate were evaluated with standard light metallographic techniques on samples etched in nital. To evaluate the effect of aging time on hardness, cube samples, 1 inch square, were cut from one of the 1 inch thick plates and heat treated with the following procedure: austenitize at 900°C for 120 min.; quench into a 370°C salt bath and age for 15, 30, 45, 60, 90, and 120 min. followed by an air cool.

2.2 Phase II

The effects of strain rate and test temperature on the tensile properties of laboratory heat treated samples were evaluated on samples from the 0.5 inch. thick as-cast plates. The two plates were cut into eight equal sections, each 4 inch x 4 inch square, and six of the sections were heat treated with the following procedure: pretreatment of 90 min. at 635°C followed by a furnace cool; austenitize at 900°C for 120 min.; quench into a 345°C salt bath for 90 min. followed by an air cool. Coupons (0.5 x 0.5 x 4.0 inches) were cut for tensile samples and prior to machining the hardness was measured on each coupon; the measured values for all coupons were between 32 HRC and 38 HRC. Round tensile samples with a 1.2 inch long by 0.25 inch diameter gage section, were machined from the heat treated coupons. The gage sections were ground to an 8 μ-inch finish.

Tensile tests were performed on a screw-driven testing machine at -80, -30, 23, 70, and 120 °C and a constant crosshead speed of 0.02 in/min. The

test system was equipped with a special test frame which allowed the samples to be submerged in heating or cooling fluids (7). For tensile testing at -80 and -30°C, temperature was maintained with a controlled refrigerated alcohol bath. The 23°C tests were performed in air and the elevated temperature tests were performed in a constant temperature oil bath. Strain was directly measured with a submersible extensometer attached to the tensile samples and load-strain tensile data were recorded on a computer-based data acquisition system. Selected tests at 23°C were also performed at 0.2 in/min. At least three samples were tested at each test condition. The microstructures were evaluated in the as-polished condition on as-received samples and sections through the tensile fracture surfaces. The graphite nodule size distributions and average sizes were determined from polished samples with a Leco image analyzer.

2.3 Phase III

Four 8 inch x 8 inch square plates were received commercially heat treated to either Grade 1 properties with an average hardness of 33 HRC or Grade 3 properties with an average hardness of 42 HRC as specified by ASTM 897-90 (5). For each heat treated condition, one plate was 0.5 inch thick and one was 1.0 inch thick. Tensile tests were performed with the same procedures outlined for Phase II above.

As part of Phase III, retained austenite measurements were obtained on all samples. An approximate method, based on x-ray diffraction measurements, as calibrated against the volume fraction of a "known" samples in which the austenite volume percent was obtained from Mossbauer measurements, was utilized. The specific procedures were as follows: obtain as a calibration sample a laboratory heat treated coupon with a high volume fraction of retained austenite; measure the retained austenite content on the calibration sample with Mossbauer spectroscopy; for the calibration sample and each test sample obtain the x-ray diffraction pattern for a scan from approximately 2θ of 60° to 80° and determine the peak height intensities for the (200) ferrite peaks (I_α) and the (220) austenite peaks (I_γ); for each test sample determine the apparent volume fraction of austenite, $f_{\gamma\text{-app}}$, defined as $I_\gamma/(I_\alpha + I_\gamma)$; for the calibration sample determine the ratio of the actual austenite volume fraction (as obtained from Mossbauer measurements) to $f_{\gamma\text{-app}}$ and define this ratio as a calibration factor β; finally determine the actual volume fraction, f_γ, defined as β x $f_{\gamma\text{-app}}$. It was estimated that this technique will predict an austenite volume fraction within about 10% of the quoted level (e.g. $f_\gamma = 20\% \pm 2\%$).

To evaluate the effects of strain on austenite transformation during deformation at room temperature, samples of the 0.5 inch thick plates of both the Grade 1 and Grade 3 materials were deformed by rolling on a laboratory rolling mill.

3.0 RESULTS

3.1 Phase I

Light micrographs of the as-cast microstructures are shown in Fig. 1. Figures 1a and 1b present two magnifications of the 0.5 inch thick plate and Figs. 1c and 1d present corresponding results for the 1 inch plate. The as-cast microstructures are independent of plate thickness and consist of spherical graphite nodules surrounded by ferrite in a pearlitic matrix. The effects of time during austempering at 370°C on the heat treated microstructures for samples austempered for 15, 45, 60, and 120 minutes are shown in Fig. 2 and on hardness are shown in Fig. 3. The heat treated microstructures are essentially independent of time and consist of graphite nodules in a matrix of acicular ferrite and austenite. This matrix microstructure is sometimes referred to as "ausferrite" (2). Figure 3 shows that the hardness is high for the 15 minute austempered sample and is essentially constant for all other tempering times. Also shown in Fig. 3 is the effect of austempering time on samples of an 1.5 pct Ni-0.3 pct Mo alloy heat treated at 900°C (10). A similar high hardness for short times and hardnesses which are essentially independent of time for longer times were obtained for both alloys.

3.2 Phase II

The laboratory heat treated samples exhibited smooth tensile stress-strain curves with minimal variability in measured flow stresses but with significant variability in total ductility. As an example, Fig. 4 presents four stress-strain curves for samples tested at 120°C and 0.02 in/min. The total ductility varied between 1.9 and 20%.

The effects of test temperature on the tensile stress-strain behavior for samples deformed at 0.02 in/min are shown in Fig. 5. Results for the samples with the highest ductility at a given test temperature have been selected. In general, with a decrease in temperature, the peak ductility decreased and the strength increased. The results of the tensile tests performed in Phase II are summarized in Table 2 which includes the yield strengths at an offset strain of 0.2%, ultimate tensile strengths, tensile ductilities, reduction in areas at fracture, and the average sample hardnesses. For these samples at least 5 hardness tests were obtained within the grip section of each tensile sample; the typical total variation in hardness within one sample was approximately 3 HRC units.

Selected results of the Phase II metallography study on deformed tensile samples are presented in Figs. 6 and 7. Figure 6 includes micrographs which show cross sections of tested tensile samples. The micrographs were obtained at a location adjacent to the fracture surfaces which are evident at the top of each micrograph. The microstructure consists of graphite nodules, microporosity, and microcracks. The micrographs illustrate the range in graphite nodule distributions observed in this study. For samples which exhibited low ductilities, the microcracks are associated with the microporosity. However, for samples which exhibited high ductilities,

microcracks also nucleated at graphite nodules.

In Fig. 7, quantitative metallographic analysis of the graphite nodule size distributions for the four micrographs in Fig. 6 are presented. In each bar chart the dashed line indicates the average nodule size distribution for all of the samples. For the micrographs shown here, the sample shown in Fig. 7b (and Fig. 6b) exhibits a size distribution which is similar to the average. In contrast, Fig. 7c (and Fig. 6c) shows a sample with a higher density of large graphite particles while the sample in Fig. 7d (and Fig. 6d) shows a higher density of fine particles.

3.3 Phase III

Tensile properties of the commercially heat treated samples tested at 0.02 in/min are summarized in Tables 3 to 6 for the Grade 1 (33 HRC) and Grade 3 (42 HRC) materials. Each table includes data for one heat treat grade and plate thickness. Data include yield strength, ultimate tensile strength, total tensile elongation, and reduction in area at fracture. Representative tensile curves for the Grade 1 and Grade 3 materials are presented in Figures 8 to 11. In each figure stress-strain curves for the samples which exhibited the maximum ductility at each test temperature in the temperature range of -80°C to 120°C are presented. Also, each figure includes a presentation of the complete stress strain curves in part "a" and in part "b" a plot on an expanded strain scale to illustrate the effects of temperature on the onset of yielding. All samples exhibited continuous yielding behavior. As shown in Figs. 8 and 9 for the Grade 1 material, the deformation behavior is essentially independent of plate thickness but depends on test temperature. At -80°C the Grade 1 material exhibits a low yield strength and a high initial strain hardening rate. With an increase in test temperature, the yield stress increases and the initial strain hardening rate decreases. In contrast, for the Grade 3 material the deformation behavior is essentially independent of plate thickness and test temperature.

The effects of test temperature on tensile properties are summarized in Figs. 12 and 13 in which the yield stresses and ultimate tensile strengths for each grade type and plate thickness are plotted versus test temperature. Figures 12a and 12b show that for the Grade 1 material the yield stress increases with test temperature while the ultimate tensile strengths are essentially independent of test temperature. In contrast to the Grade 1 material, Figures 13a and 13b show that for the Grade 3 material there is no apparent temperature dependence of either the yield stress or ultimate tensile strengths.

3.4 Analysis of Retained Austenite

Retained austenite measurements were made on the as heat treated materials for each experimental phase and as a function of imposed rolling strain for samples of the Grade 1 and Grade 3 materials in Phase III. The retained austenite measurements on the heat treated samples are summarized in Table 7. In Phase I for the samples austempered at 370°C the retained

austenite volume fractions were essentially constant in the range of 20 to 25%. The material austempered at 345°C in Phase II exhibited approximately 38% austenite while the Grade 1 and Grade 3 materials of Phase III exhibited volume fractions of 27 and 19% respectively. Also shown in Table 7 is the retained austenite measured on a sample removed from a tank track section.

The effects of imposed rolling strain on strain-induced transformation of austenite in the Grade 1 and Grade 3 materials of Phase III are shown in Figure 14. For both materials the volume fraction of austenite decreased with an increase in strain. Also, at high strains both materials exhibited essentially the same retained austenite content of approximately 6% for samples strained 19% by rolling. This deformation-induced transformation of austenite documented in the rolling experiments is expected.

4.0 DISCUSSION

Figure 15 summarizes all combinations of ultimate tensile strengths and elongations for ADI specimens tested in the Phase II and Phase III experiments of this investigation. The data are compared to a band of expected ultimate tensile strength-elongation combinations for ADI published by Gundlach and Janowak (1). The lower boundary of the band corresponds to minimum values of room temperature properties tabulated for ADI specimens in the ADI ASTM specification and summarized in Table 1 (4). While the Grade 1 and Grade 3 ultimate strengths measured in this investigation generally meet the requirements of the ASTM specification, the elongations of most specimens are below the expected values.

There may be a number of explanations for the lower than expected ductilities of the ADI specimens. Documented variations in nodule size distributions and microporosity are possible causes of fracture initiation and reduced elongation. Segregation at intercell boundaries, which leads to large volumes of unreacted austenite and to reduced ductility, does not appear to be a factor in the specimens examined in this study. Another factor which might account for reduced ductility is the effect of low-temperature testing as described below.

Apart from ductility, the flow strengths and strain hardening behavior of the ADI specimens are significantly affected by test temperature. In specimens with high retained austenite contents, yield strength decreases with decreasing test temperature in contrast to the behavior of specimens with stable microstructures. The reduced yield strengths are associated with the strain-induced austenite transformation to martensite, a process that, because of the associated volume increase, increases the effective strain measured during yielding (11). However, as shown in Figure 8, the strain-induced martensite causes rapid strain hardening and increased strain hardening at low plastic strains. The latter behavior is most pronounced in the Grade 1 specimens with high retained austenite. In Grade 3 specimens with lower retained austenite, yielding behavior is effectively insensitive to testing temperature, Figure 13.

At higher testing temperatures, the mechanical stability of the retained austenite increases, and there is little effect of austenite transformation on yield behavior. However, with increasing strain the austenite eventually transforms, and if the strain-induced transformation occurs around the point of necking instability, the enhanced strain hardening effectively defers necking and increases ductility (6-9). The latter effect appears to be operating in the specimens tested above room temperature where the highest elongations measured in this investigation were observed.

In addition to a change in strain hardening behavior, the fracture mode in the ferrite between graphite nodules changed with test temperature from void coalescence at high temperatures to cleavage at temperatures at or below -30°C. To illustrate this point, Fig. 16 presents SEM photographs of the tensile fracture surfaces of Phase II samples tested at 120°C (Fig. 16a) and -30°C (Fig. 16c). Also shown in Figs. 16b and 16d are the corresponding cross sections of the fracture surfaces (similar to those presented in Fig. 6)

for the 120°C and -30°C samples respectively. The fracture of the 120°C sample is associated with well defined void coalescence (Fig. 16a) and necking (Fig. 16b). In contrast, fracture of the -30°C sample exhibits cleavage in the matrix (Fig. 16c) and a relatively flat fracture surface with limited necking (Fig. 16d). Since Fig. 15 includes all of the data of this study, while the ASTM results are for room temperature tests, the transition to cleavage fracture at low temperatures may contribute to the decreased ductilities observed in the samples of this study in comparison to the minimum values quoted by ASTM.

5.0 CONCLUSIONS

1. The temperature dependence of the strain-induced transformation of retained austenite to martensite in ADI specimens plays an important role in establishing deformation behavior.

2. At low testing temperatures, the strain-induced transformation of retained austenite occurs at low strains, reduces yield strengths, and increases strain hardening rates at low strains.

3. At high testing temperatures, the strain-induced transformation of retained austenite occurs at high strains and the associated increases in strain hardening increase ductility.

4. There is a transition in fracture mode of the ADI matrix from ductile to brittle as test temperature is decreased below room temperature.

4. The elongations measured for ADI specimens except for specimens tested above room temperature, were generally lower than expected. The lower ductilities were related to microporosity, differences in graphite nodule distributions, and a transition in strain hardening and fracture behavior at low testing temperatures. Further work is necessary to develop detailed correlations of microstructure with fracture phenomena of ADI.

6.0 ACKNOWLEDGEMENTS

The authors acknowledge the discussions and assistance of Dr. Mani of Wagner Casting Company, Decator, Illinois. The assistance of Dr. Dong Won Oh with the testing is greatly appreciated.

7.0 REFERENCES

1. R.B. Gundlach and J.F. Janowak, "A Review of Austempered Ductile Iron Metallurgy", in First International Conference on Austempered Ductile Iron, American Society for Metals, Metals Park, OH, 1984,p. 1-12.

2. B.V. Kovacs, Sr., "Austempered Ductile Iron - Fact and Fiction", Modern Castings, vol. 80, no. 3, March, 1990, pp. 38-41.

3. B.V. Kovacs, Sr., "A Simple Technique to Identify Various Phases in Austempered Ductile Iron," Modern Castings, vol. 77, no. 6, 1987, pp. 34-35.

4. D.J. Moore, T.N. Rouns, and K.B. Rundman, "The Relationship Between Microstructure and Tensile Properties in Austempered Ductile Irons", AFS Transactions, vol. 95, 1987, pp. 765-774.

5. "Austempered Ductile Iron Castings," ASTM Specification No. A 897-90.

6. Y. Sakuma, D.K. Matlock, and G. Krauss, "Intercritically Annealed and Isothermally Transformed 0.15 pct C Steels Containing 1.2 pct Si-1.5 pct Mn and 4 pct Ni: Part I. Transformation Microstructure, and Room Temperature Mechanical Properties", Metallurgical Transactions A, vol. 23A, 1992, pp. 1221-1232.

7. Y. Sakuma, D.K. Matlock, and G Krauss, "Intercritically Annealed and Isothermally Transformed 0.15 pct C Steels Containing 1.2 pct Si-1.5 pct Mn and 4 pct Ni: Part II. Effect of Testing Temperature on Stress-Strain Behavior and Deformation-Induced Austenite Transformation", Metallurgical Transactions A, vol. 23A, 1992, pp. 1233-1241.

8. W.C. Jeong, D.K. Matlock, and G. Krauss, Materials Science and Engineering 1993, "Observation of Deformation and Transformation Behavior of Retained Austenite in a 0.14 pct C - 1.2 pct Si - 1.5 pct Mn Steel with Ferrite-Bainite-Austenite Structure", Materials Science and Engineering, vol. A165, 1993, pp. 1-8.

9. W.C. Jeong, D.K. Matlock, and G. Krauss, "Effects of Tensile Testing Temperature on Deformation and Transformation Behavior of Retained Austenite in a 0.14 pct C - 1.2 pct Si - 1.5 pct Mn Steel with Ferrite-Bainite-Austenite Structure", Materials Science and Engineering, vol. A165, 1993, pp. 9-18.

10. J.F. Janowak and P.A. Morton, "A Guide to Mechanical Properties Possible by Austempering 1.5%No-0.3%Mo Ductile Iron", Report No. XGI-84-03, Amax Materials Research Center, Ann Arbor, Michigan, 1984.

11. K.J. Grassl, S.W. Thompson, D.K. Matlock, and G. Krauss, "Toughness of Medium-Carbon Forging Steels with Direct Cooled Bainitic Microstructures", 31st Mechanical Working and Steel Processing Conference Proceedings, vol. 27, Chicago, Illinois, October 22-25, 1989, ISS-AIME, Warrendale, PA, 1990, pp. 137-143.

TABLE 2 - Summary of Sample Designations, Test Conditions, and Tensile Properties for All Tensile Samples in Phase II

SPECIMEN NO.	TEST TEMP. (°C)	CROSSHEAD SPEED (in/min)	YIELD POINT (ksi)	ULTIMATE STRENGTH (ksi)	ELONGATION (%)	REDUCTION IN AREA (%)	AVERAGE HARDNESS HRC
ADI5	-80	0.02	86	132	2.4	1.2	35.0
ADI8	-80	0.02	103	141	3.0	1.6	37.9
ADI22	-80	0.02	95	109	4.3	1.6	36.2
ADI34	-80	0.02	118	163	4.6	2.0	36.5
ADI1	-30	0.02	110	125	1.4	0.8	35.8
ADI12	-30	0.02	108	131	2.3	1.6	35.1
ADI25	-30	0.02	103	121	3.1	1.6	35.9
ADI16	-30	0.02	111	130	1.5	0.8	35.9
ADI7	23	0.02	109	142	4.6	2.0	35.8
ADI15	23	0.02	107	140	7.9	N/A	35.0
ADI28	23	0.02	104	142	12.1	4%	34.0
ADI3	23	0.2	115	140	2.6	N/A	36.3
ADI17	23	0.2	108	133	4.3	N/A	35.1
ADI36	23	0.2	110	155	11.0	N/A	35.5
ADI27	70	0.02	104	137	7.3	3.6	35.6
ADI39	70	0.02	103	134	4.3	2.8	35.5
ADI13	120	0.02	110	134	1.9	2.4	35.4
ADI21	120	0.02	110	153	14.9	6.0	35.4
ADI29	120	0.02	115	148	5.1	3.6	35.5
ADI38	120	0.02	107	152	20.0	8.0	35.4

TABLE 3 - Summary of Sample Designations, Test Conditions, and Tensile Properties for All Tensile Samples in Phase III, for Grade 1 Samples from the 0.5 Inch Thick Plate

SPECIMEN NO.	TEST TEMP. (°C)	CROSSHEAD SPEED (in/min)	YIELD STRESS (ksi)	ULTIMATE STRENGTH (ksi)	TOTAL ELONGATION (%)	REDUCTION IN AREA (%)
AAA13	-80	0.02	90	133	3.2	1.6
AAA14	-80	0.02	85	139	3.5	1.6
AAA15	-80	0.02	81	121	2.0	0.8
AAA10	-30	0.02	103	146	5.0	2.0
AAA11	-30	0.02	104	137	3.6	1.6
AAA12	-30	0.02	105	131	2.7	1.2
AAA1	23	0.02	109	150	---	4.8
AAA2	23	0.02	109	148	11.1	3.6
AAA3	23	0.02	108	140	6.3	2.0
AAA16	70	0.02	105	137	7.1	3.2
AAA5	70	0.02	111	137	4.6	2.4
AAA6	70	0.02	110	137	4.7	2.4
AAA7	120	0.02	105	132	4.0	1.6
AAA8	120	0.02	105	137	6.3	2.4
AAA9	120	0.02	107	147	13.7	5.0

TABLE 4 - Summary of Sample Designations, Test Conditions, and Tensile Properties for All Tensile Samples in Phase III, for Grade 1 Samples from the 1.0 Inch Thick Plate

SPECIMEN NO.	TEST TEMP. (°C)	CROSSHEAD SPEED (in/min)	YIELD STRESS (ksi)	ULTIMATE STRENGTH (ksi)	TOTAL ELONGATION (%)	REDUCTION IN AREA (%)
AAA53	-80	0.02	71	157	5.3	1.2
AAA54	-80	0.02	71	142	3.8	0.4
AAA55	-80	0.02	71	136	3.7	1.2
AAA50	-30	0.02	93	144	5.6	2.2
AAA51	-30	0.02	89	145	5.4	2.0
AAA52	-30	0.02	91	140	4.3	1.6
AAA41	23	0.02	109	141	6.4	2.4
AAA42	23	0.02	104	133	5.4	1.6
AAA43	23	0.02	103	130	4.5	1.6
AAA44	70	0.02	106	130	4.5	2.8
AAA56	70	0.02	101	126	4.9	2.0
AAA46	70	0.02	102	126	5.4	3.2
AAA47	120	0.02	103	129	4.8	1.6
AAA48	120	0.02	104	132	5.9	2.4
AAA49	120	0.02	105	139	9.9	4.0

TABLE 5 - Summary of Sample Designations, Test Conditions, and Tensile Properties for All Tensile Samples in Phase III, for Grade 3 Samples from the 0.5 Inch Thick Plate

SPECIMEN NO.	TEST TEMP. (°C)	CROSSHEAD SPEED (in/min)	YIELD STRESS (ksi)	ULTIMATE STRENGTH (ksi)	TOTAL ELONGATION (%)	REDUCTION IN AREA (%)
AAA33	-80	0.02	133	182	2.7	1.2
AAA34	-80	0.02	133	182	2.7	0.8
AAA35	-80	0.02	132	171	1.7	0.4
AAA30	-30	0.02	145	185	3.2	1.2
AAA31	-30	0.02	142	184	3.1	1.2
AAA32	-30	0.02	140	176	2.2	1.0
AAA21	23	0.02	140	190	11.3	1.6
AAA22	23	0.02	139	181	4.5	1.2
AAA23	23	0.02	126	181	---	1.2
AAA24	70	0.02	147	184	3.1	0.8
AAA25	70	0.02	148	179	2.3	0.8
AAA26	70	0.02	146	179	2.4	1.6
AAA27	120	0.02	132	173	2.7	0.8
AAA28	120	0.02	136	174	2.5	0.8
AAA29	120	0.02	138	183	6.4	2.8

TABLE 6 - Summary of Sample Designations, Test Conditions, and Tensile Properties for All Tensile Samples in Phase III, for Grade 3 Samples from the 1.0 Inch Thick Plate

SPECIMEN NO.	TEST TEMP. (°C)	CROSSHEAD SPEED (in/min)	YIELD STRESS (ksi)	ULTIMATE STRENGTH (ksi)	TOTAL ELONGATION (%)	REDUCTION IN AREA (%)
AAA73	-80	0.02	123	175	3.2	1.2
AAA74	-80	0.02	120	174	3.4	1.6
AAA75	-80	0.02	124	175	3.3	1.6
AAA70	-30	0.02	134	183	4.5	2.0
AAA71	-30	0.02	132	185	5.3	2.2
AAA72	-30	0.02	128	169	2.5	1.2
AAA61	23	0.02	138	181	5.3	1.6
AAA62	23	0.02	127	171	3.1	1.2
AAA63	23	0.02	120	167	3.5	1.2
AAA76	70	0.02	130	157	1.6	1.2
AAA77	70	0.02	131	164	2.4	1.6
AAA66	70	0.02	128	162	2.3	1.2
AAA67	120	0.02	130	168	3.2	1.6
AAA68	120	0.02	130	168	2.8	1.2
AAA69	120	0.02	125	177	---	2.2

TABLE 7 - Summary of Retained Austenite Measurements

PHASE	SPECIMENS	HARDNESS (HRC)	RETAINED AUSTENITE (%)
I	Austempered at 370°C for 15 min.	37.9	21.3
	Austempered at 370°C for 30 min.	35.0	25.2
	Austempered at 370°C for 45 min.	35.6	20.1
	Austempered at 370°C for 60 min.	34.4	23.4
	Austempered at 370°C for 120 min.	35.2	20.9
II	Austempered at 345°C for 90 min. (1st Tensile Test, Heat Treated at CSM)	32.1	38.0
III	Grade 1 (2nd Tensile Test, Commercially Heat Treated)	32.9	27.4
	Grade 3 (2nd Tensile Test, Commercially Heat Treated)	41.8	19.1
Extra	Sample from Tank	31.0	31.8

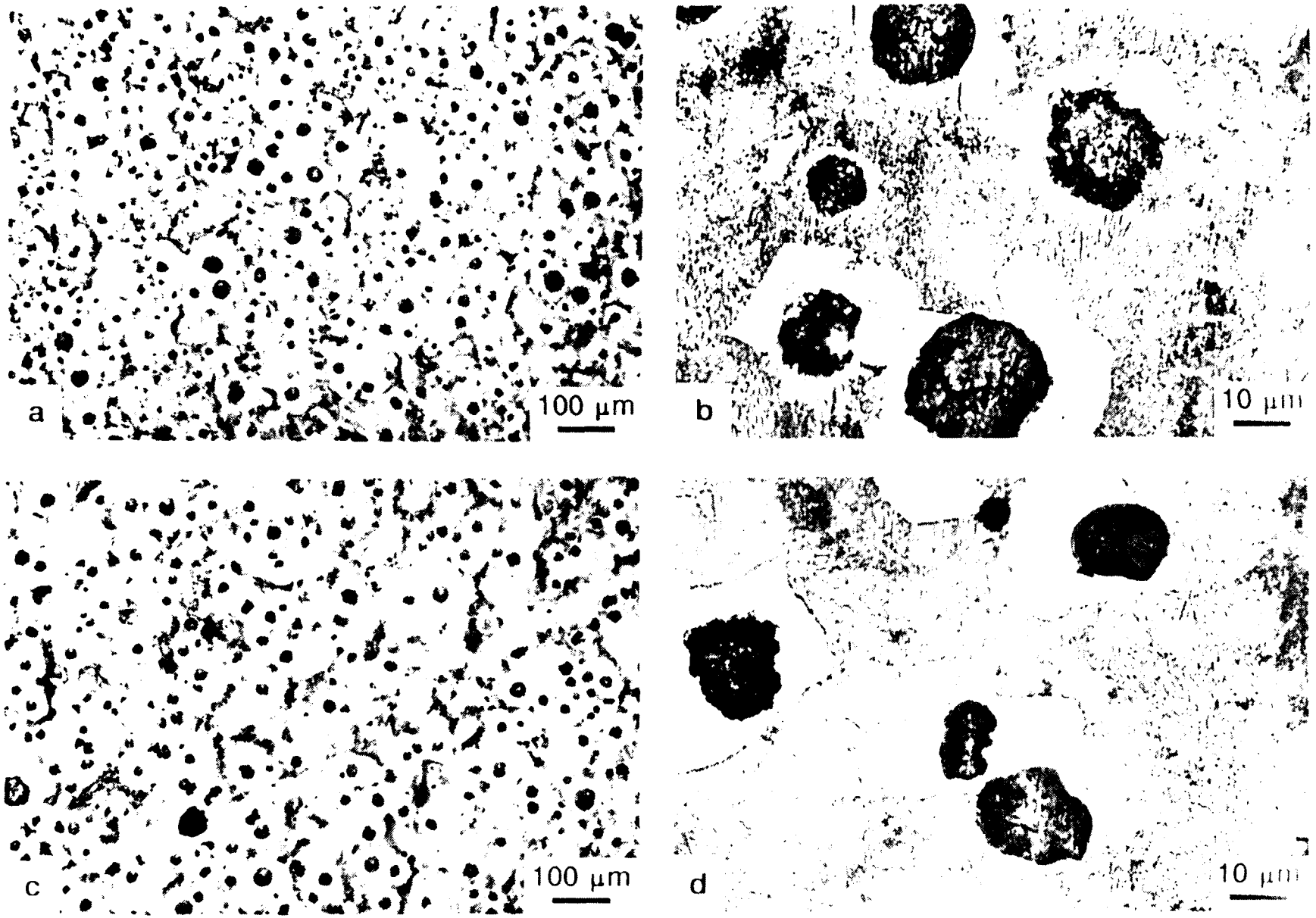

Figure 1: Microstructures of the as-cast plates. (a) 0.5 inch thick plate, 100X. (b) 0.5 inch thick plate, 1000X. (c) 1.0 inch thick plate, 100X. (b) 1.0 inch thick plate, 1000X. Light micrographs, Nital etch.

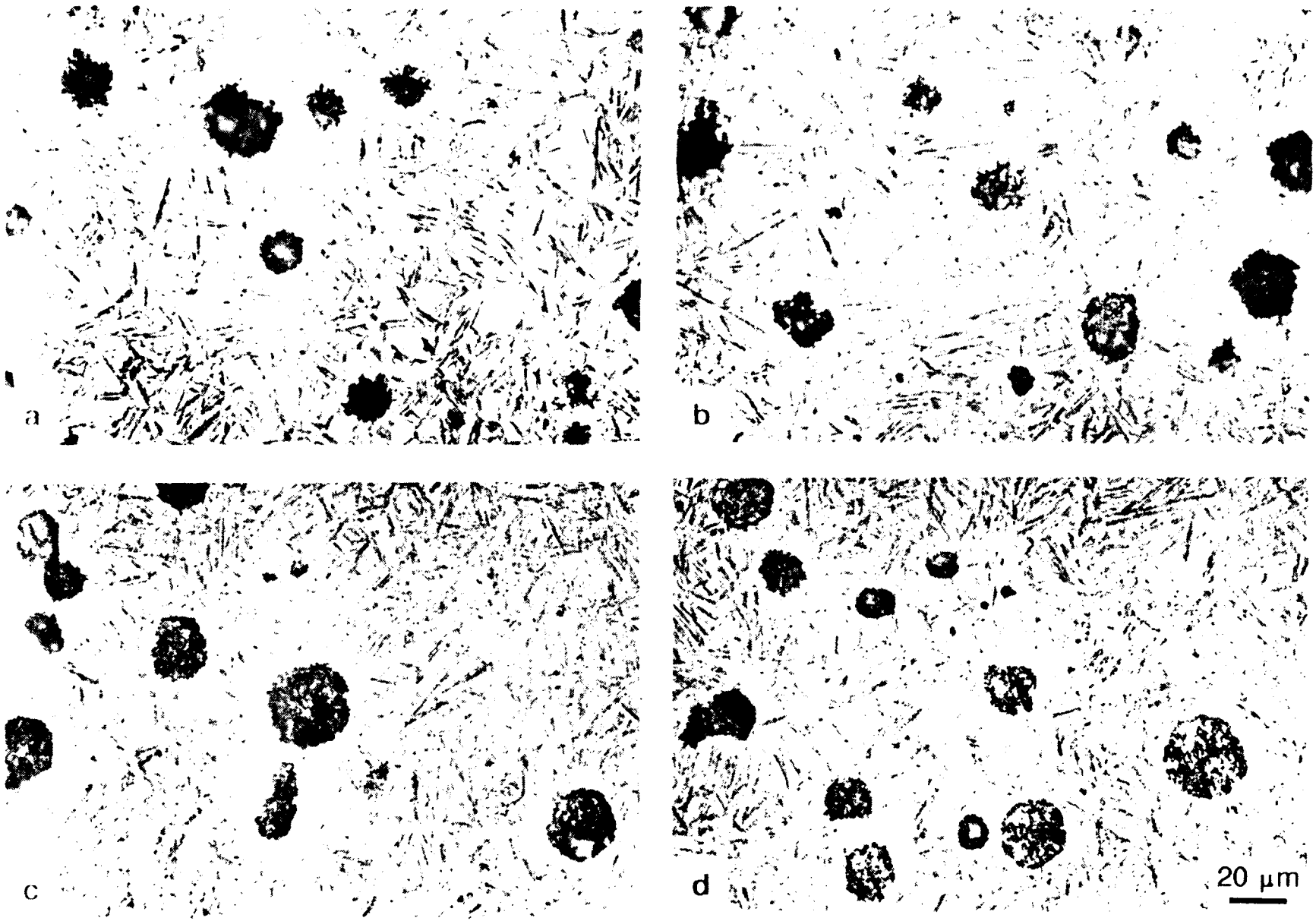

Figure 2: Microstructures of Phase I samples austempered at 370°C for: (a) 15 min. (b) 45 min. (c) 60 min. and (d) 120 min. Light micrographs, Nital etch, 500X.

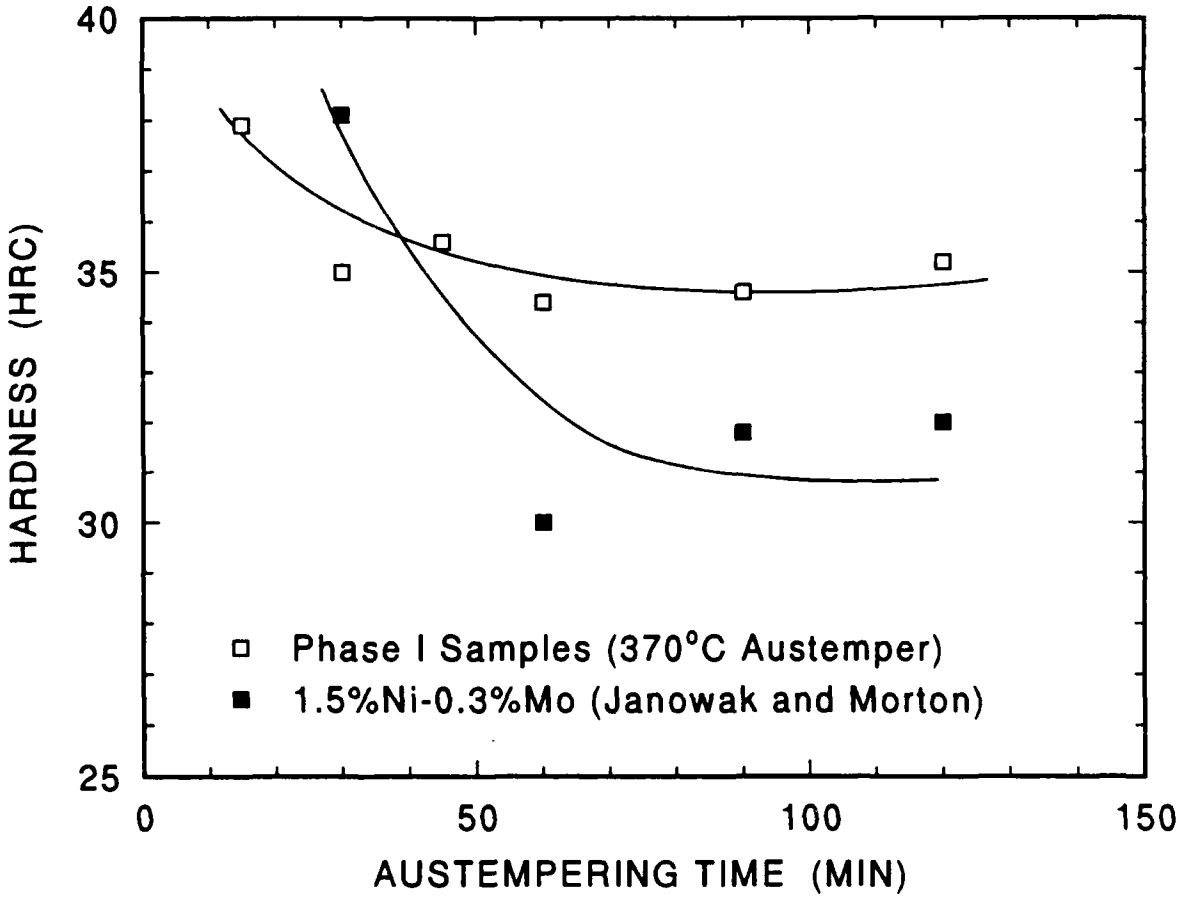

Figure 3: A summary of the effect of austempering time on the hardness of Phase I samples austempered at 370°C. Also shown are the results of Janowak and Morton (10) on 1.5%Ni-0.3%Mo alloy.

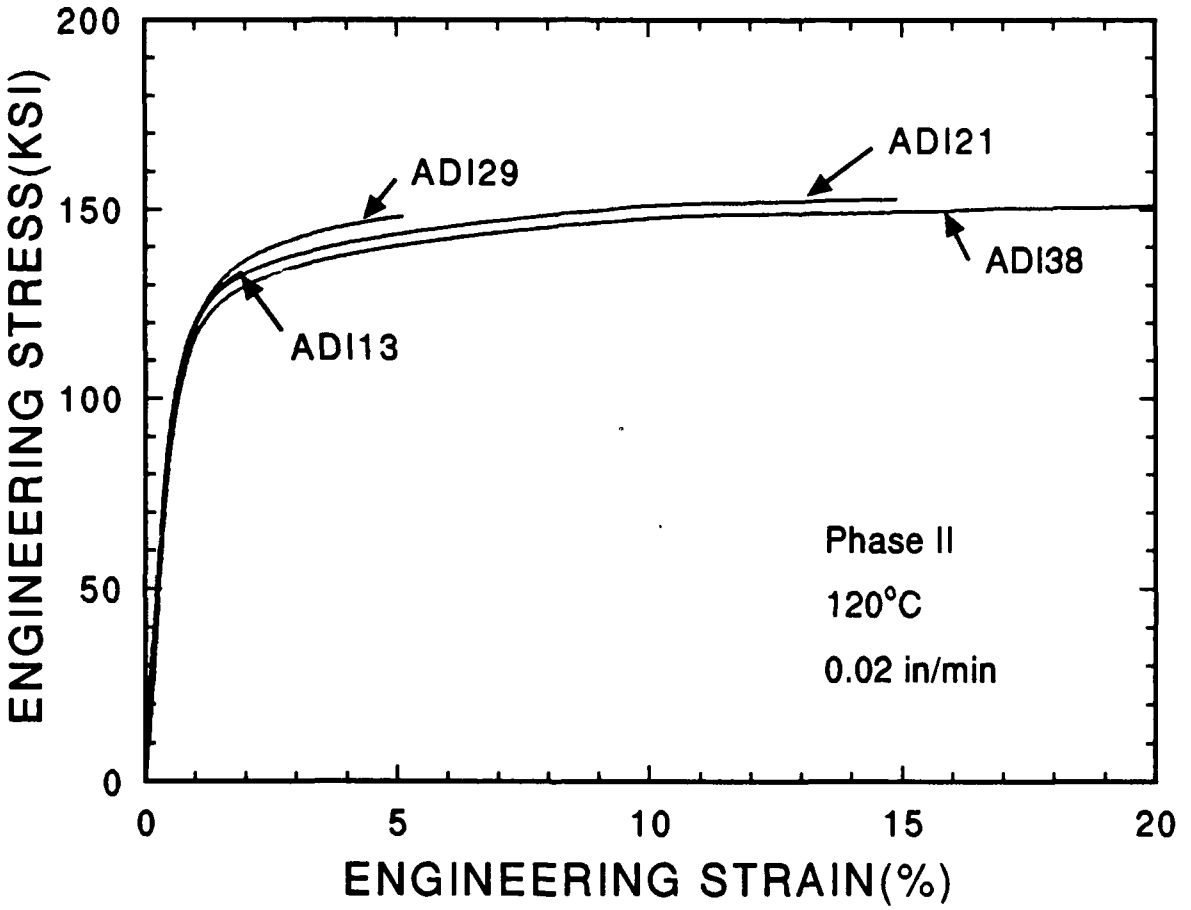

Figure 4: Tensile stress-strain curves for four Phase II samples of austenitic ductile iron tested at 120°C at a crosshead speed of 0.02 in/min.

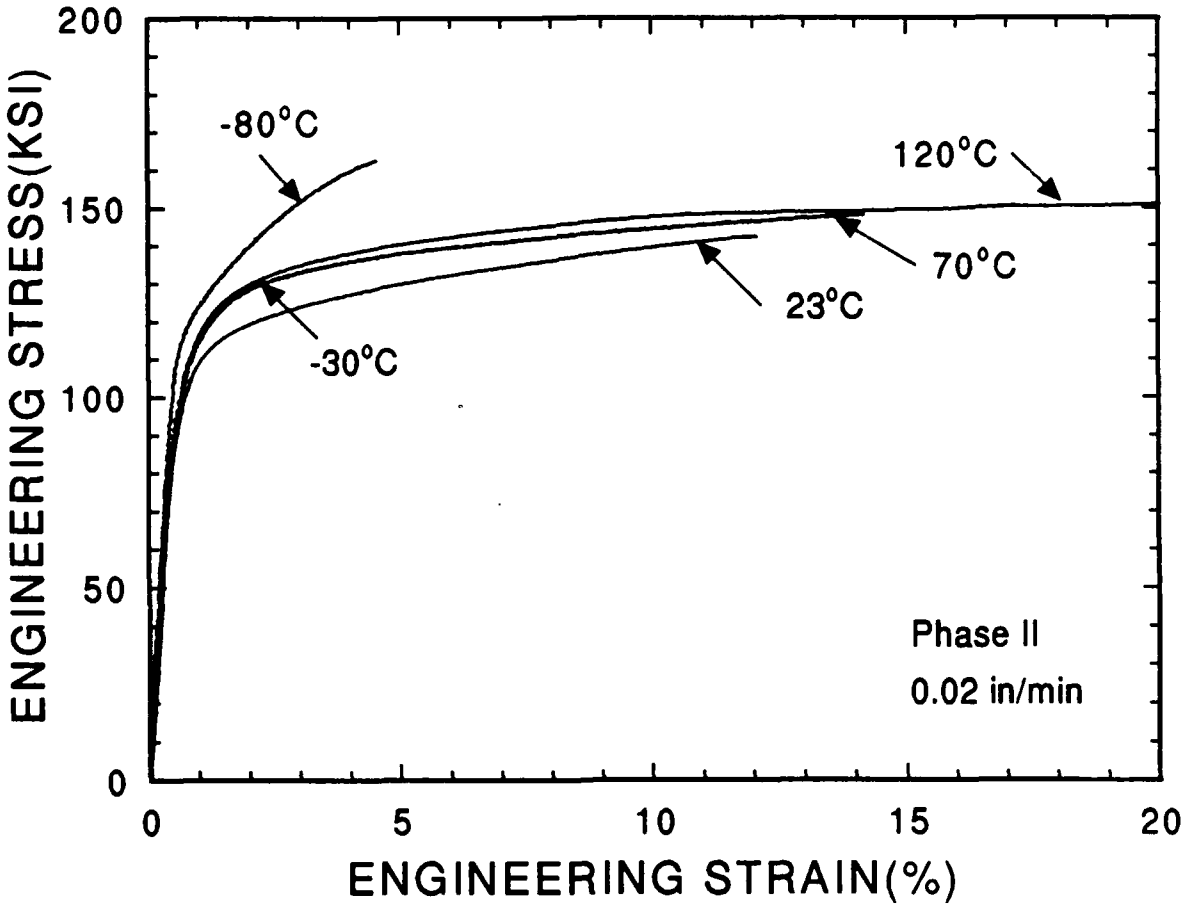

Figure 5: A comparison of the effect of test temperature on the stress-strain curves for Phase II samples which exhibited the maximum ductility at each test temperature.

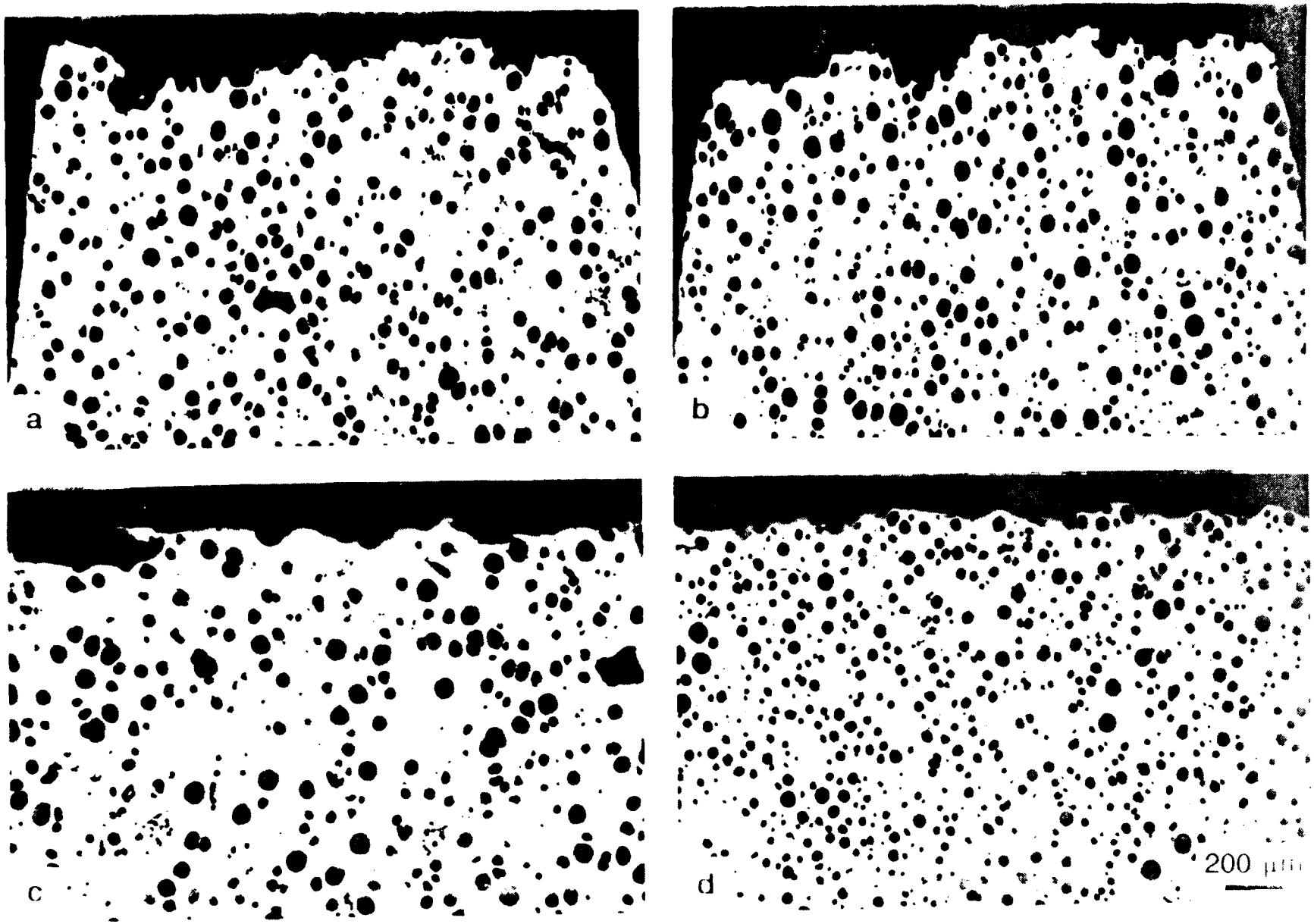

Figure 6: Selected cross sections of Phase II tensile samples; the fracture surface is visible in each photograph. (a) Sample ADI13, 120°C, 134ksi UTS, (b) Sample ADI38, 120°C, 152ksi UTS, (c) Sample ADI22, -80°C, 109ksi UTS, (d) Sample ADI34, -80°C, 163 ksi. Light micrographs, unetched.

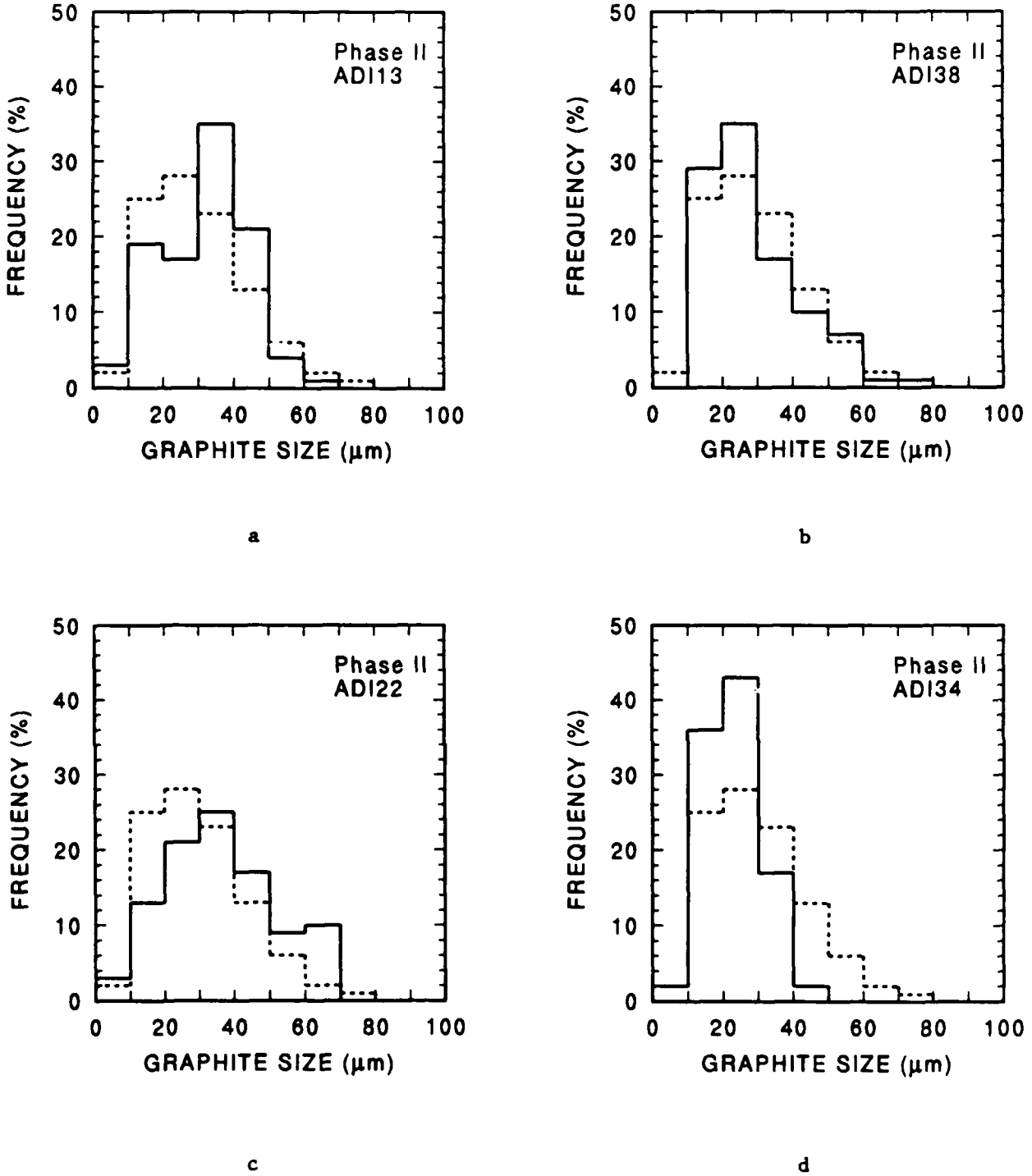

Figure 7: Graphite nodule size distributions for the Phase II micrographs shown in Figure 6. The average distribution from an analysis of 20 samples is also shown by the dashed line in each graph. (a) Sample ADI13, 120°C, 134ksi UTS, (b) Sample ADI38, 120°C, 152ksi UTS, (c) Sample ADI22, -80°C, 109ksi UTS, (d) Sample ADI34, -80°C, 163 ksi. Light micrographs, unetched.

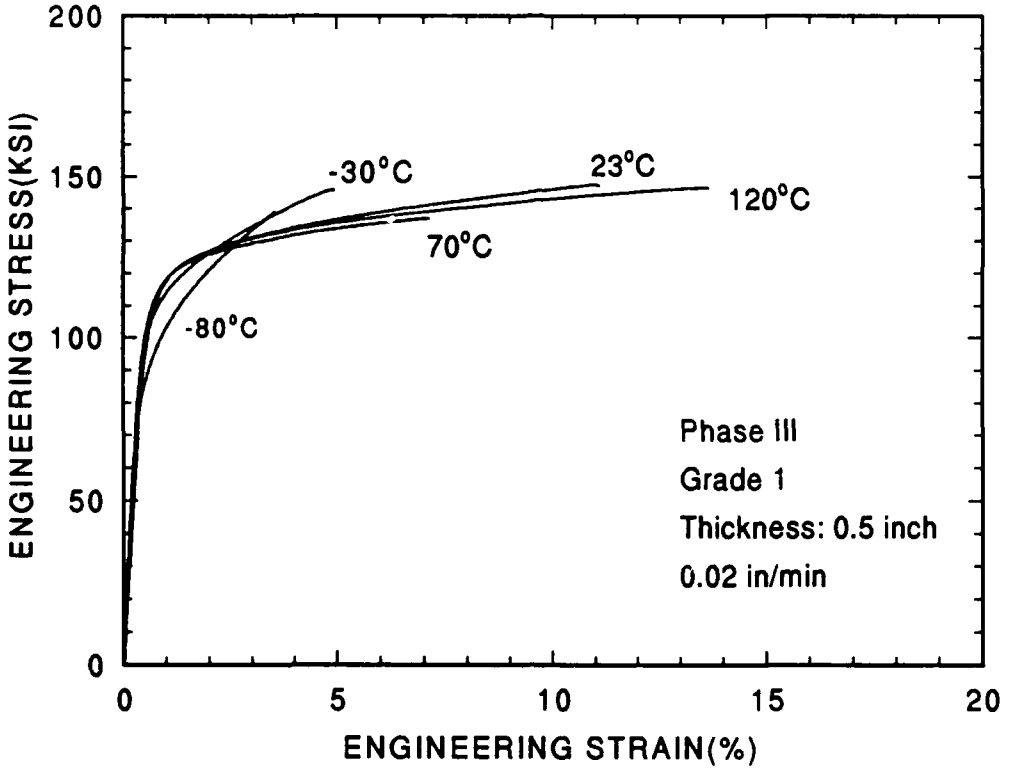

a

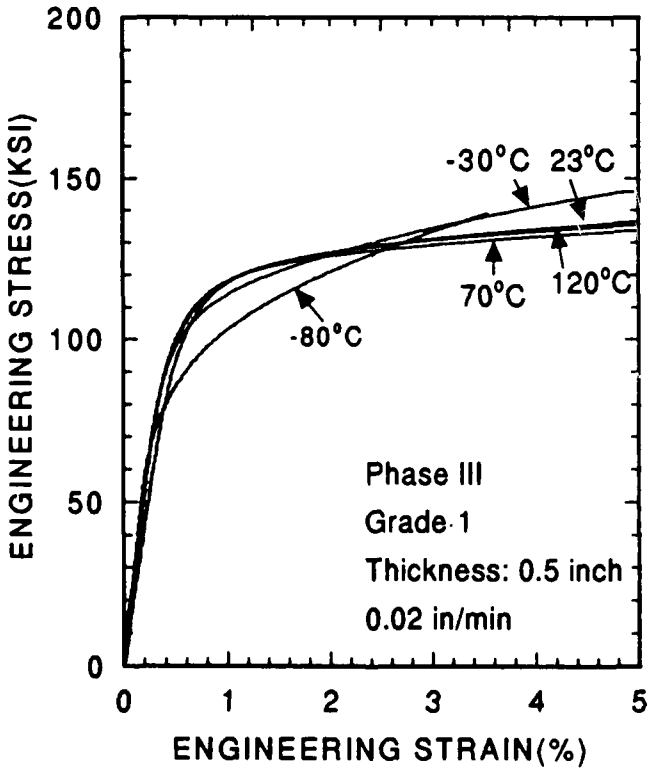

b

Figure 8: The effect of test temperature on tensile properties: Phase III, Grade 1, 0.5 inch thick plate. (a) complete stress strain curves for selected samples which exhibited the maximum ductility at each test temperature. (b) expanded low strain behavior of samples shown in part "a".

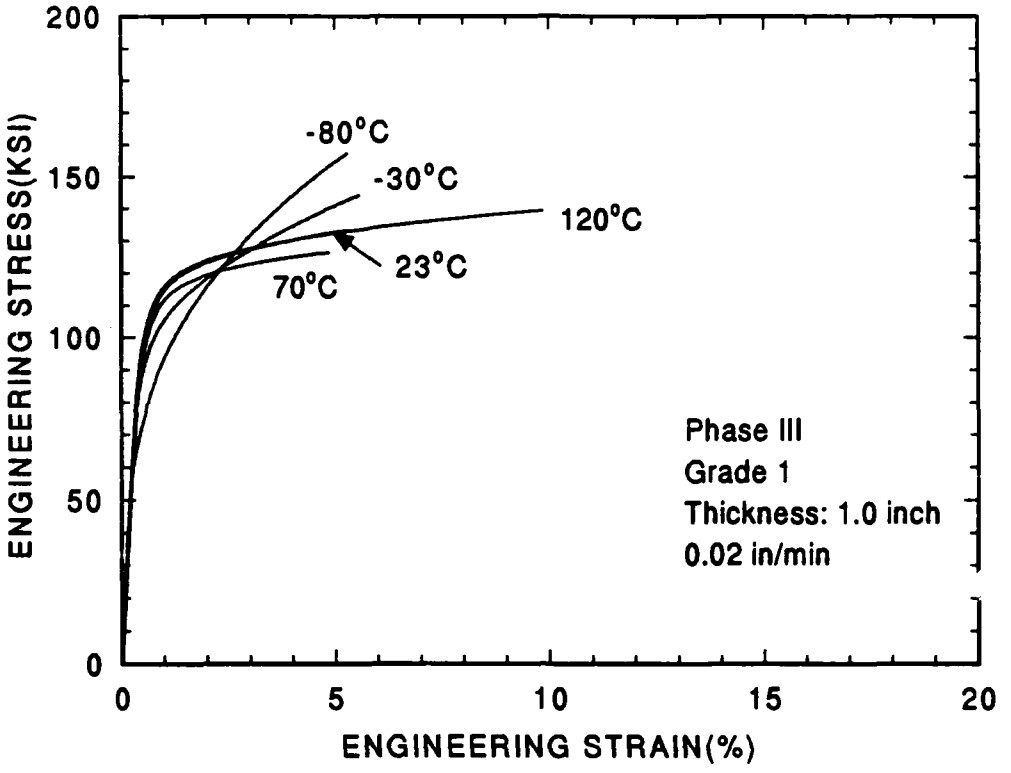

a

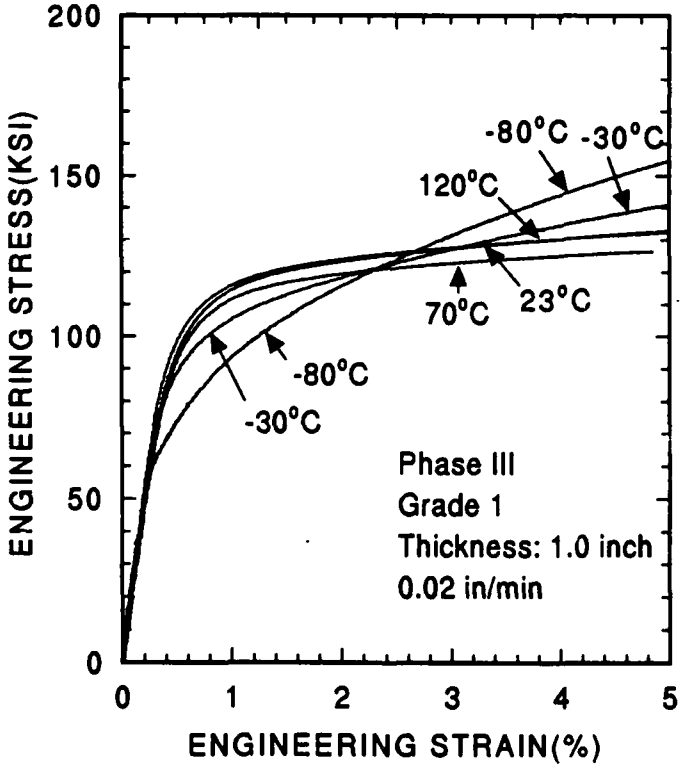

b

Figure 9: The effect of test temperature on tensile properties: Phase III, Grade 1, 1.0 inch thick plate. (a) complete stress strain curves for selected samples which exhibited the maximum ductility at each test temperature. (b) expanded low strain behavior of samples shown in part "a".

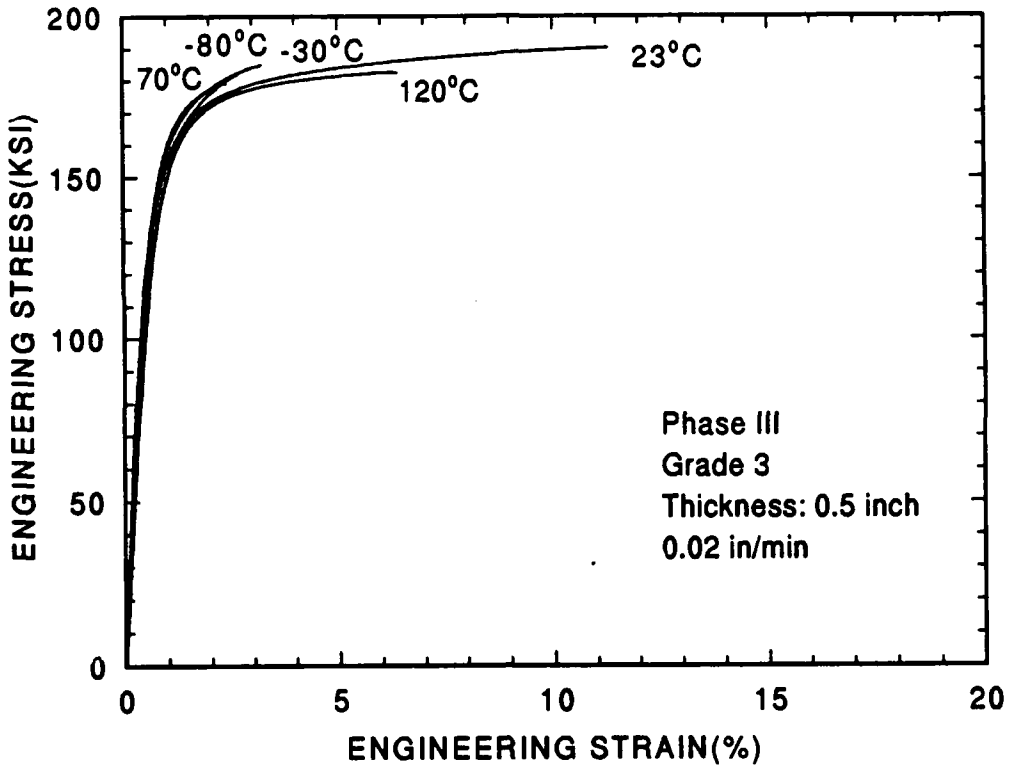

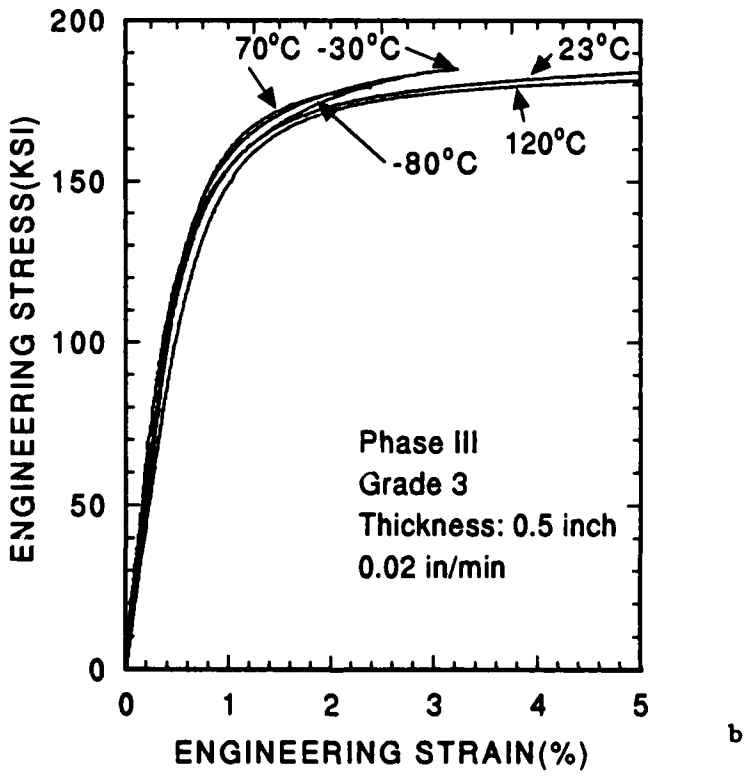

Figure 10: The effect of test temperature on tensile properties: Phase III, Grade 3, 0.5 inch thick plate. (a) complete stress strain curves for selected samples which exhibited the maximum ductility at each test temperature. (b) expanded low strain behavior of samples shown in part "a".

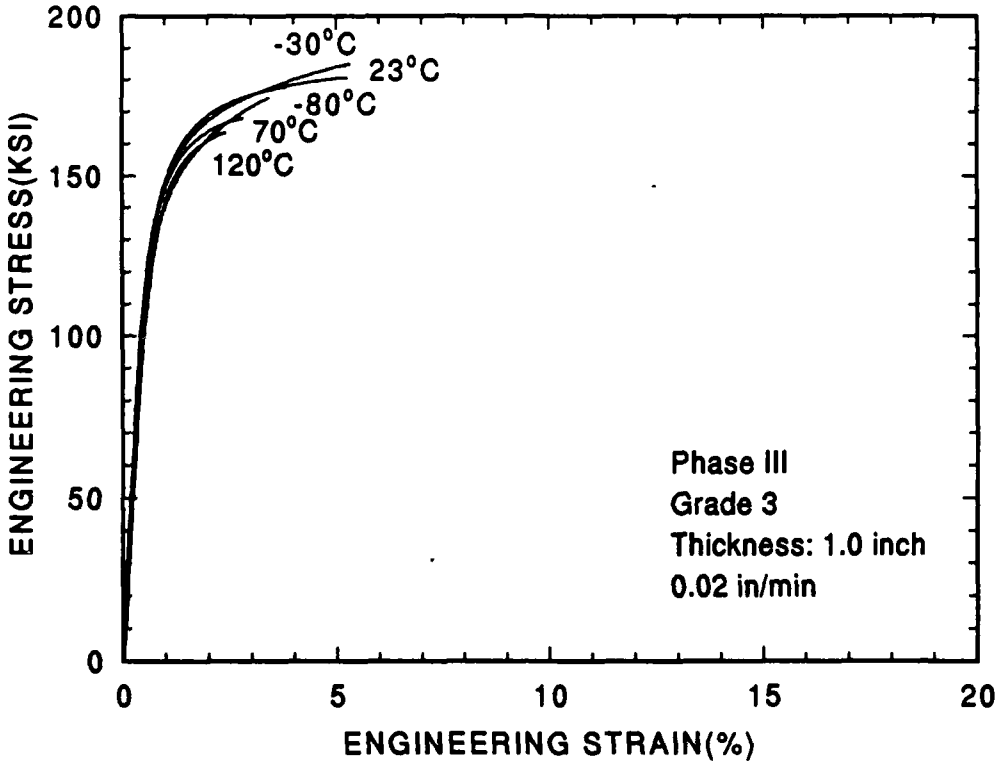

a

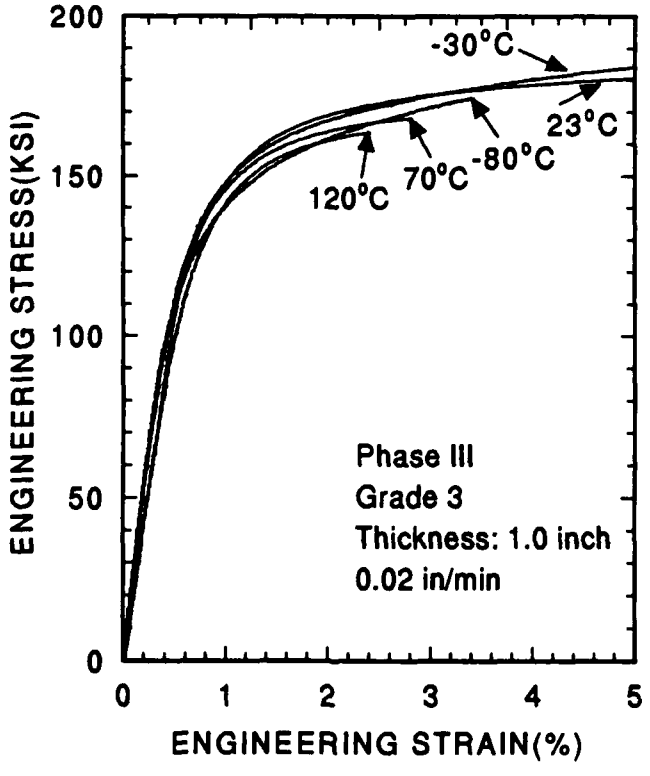

b

Figure 11: The effect of test temperature on tensile properties: Phase III, Grade 3, 1.0 inch thick plate. (a) complete stress strain curves for selected samples which exhibited the maximum ductility at each test temperature. (b) expanded low strain behavior of samples shown in part "a".

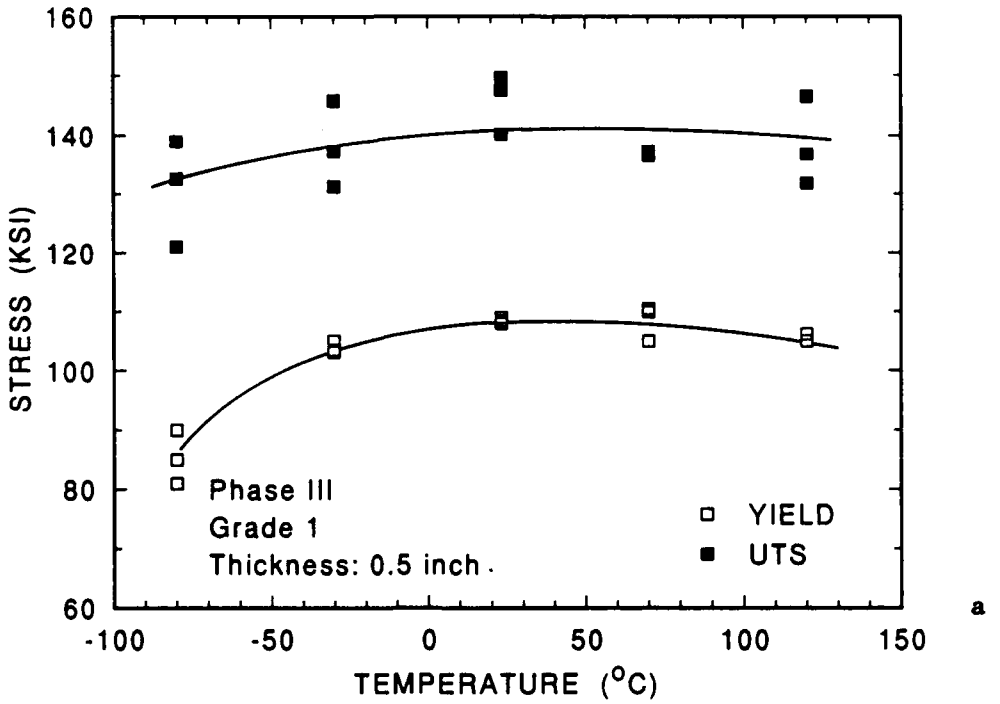

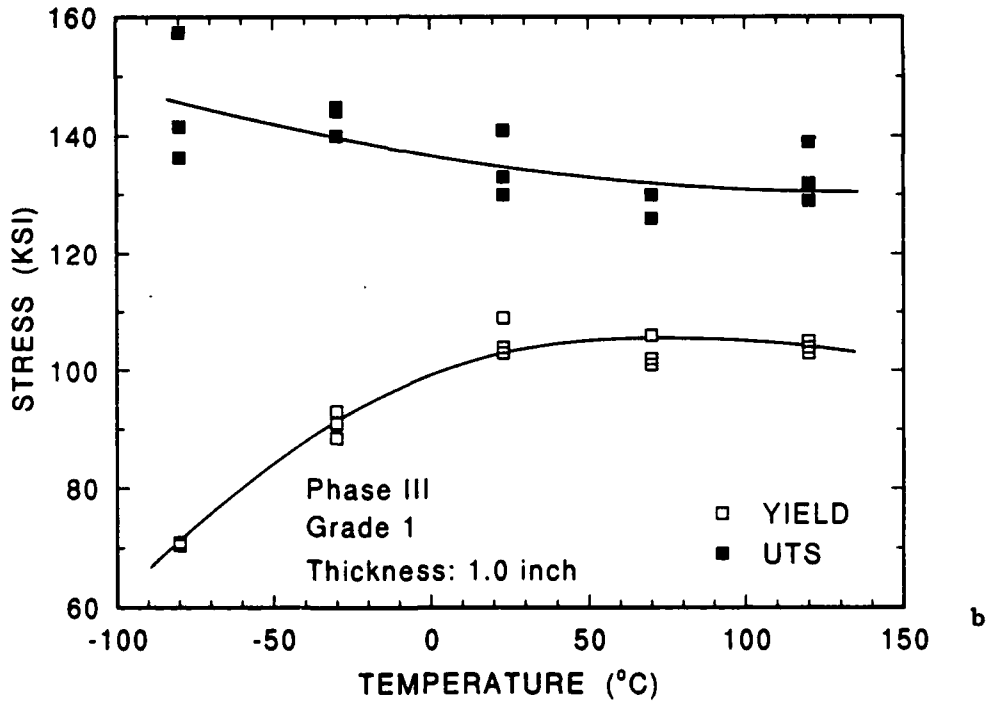

Figure 12: The effect of test temperature on the yield stress and ultimate tensile strength for all of the Phase III, Grade 1 tensile samples (a) 0.5 inch thick plate. (b) 1.0 inch thick plate.

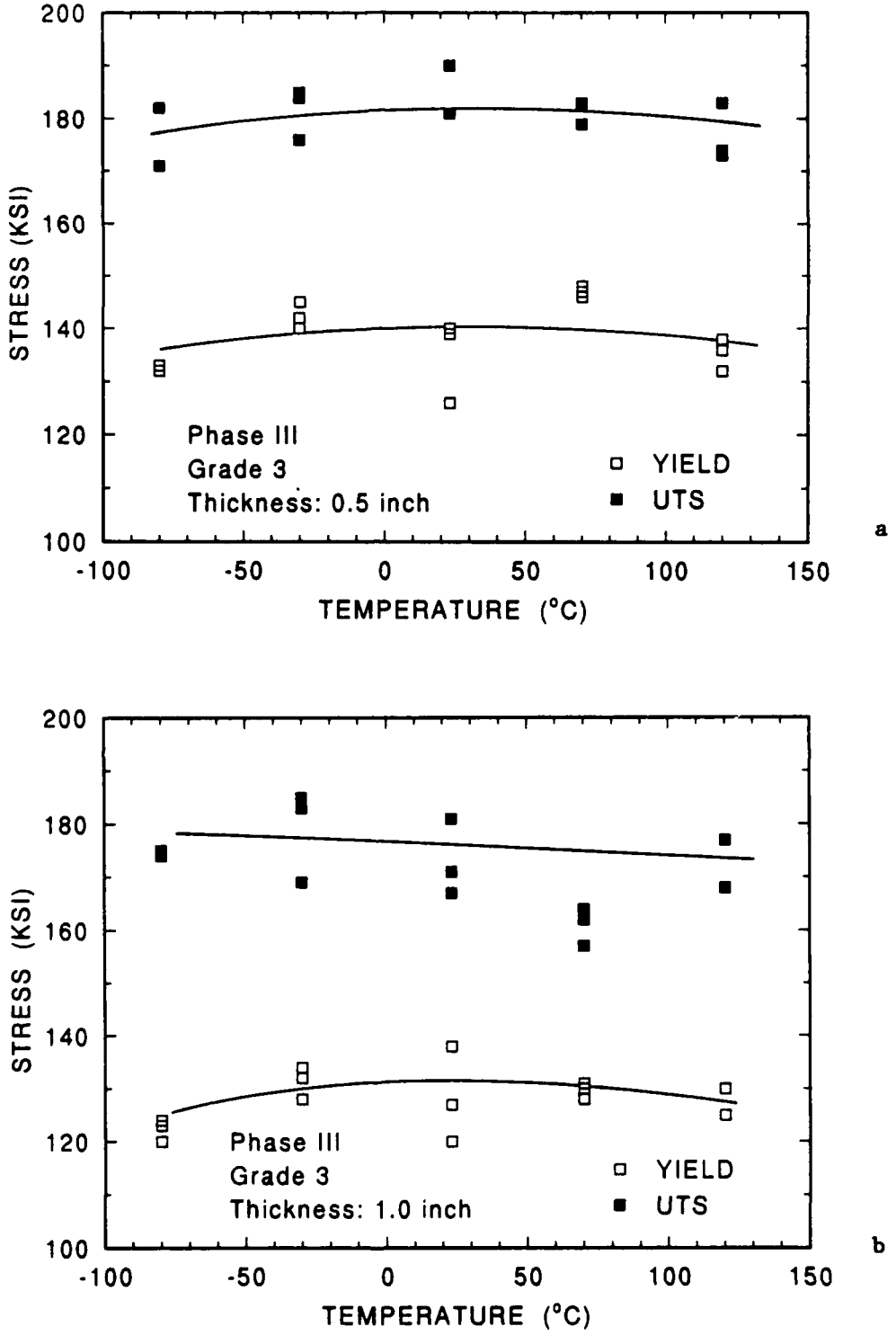

Figure 13: The effect of test temperature on the yield stress and ultimate tensile strength for all of the Phase III, Grade 3 tensile samples (a) 0.5 inch thick plate. (b) 1.0 inch thick plate.

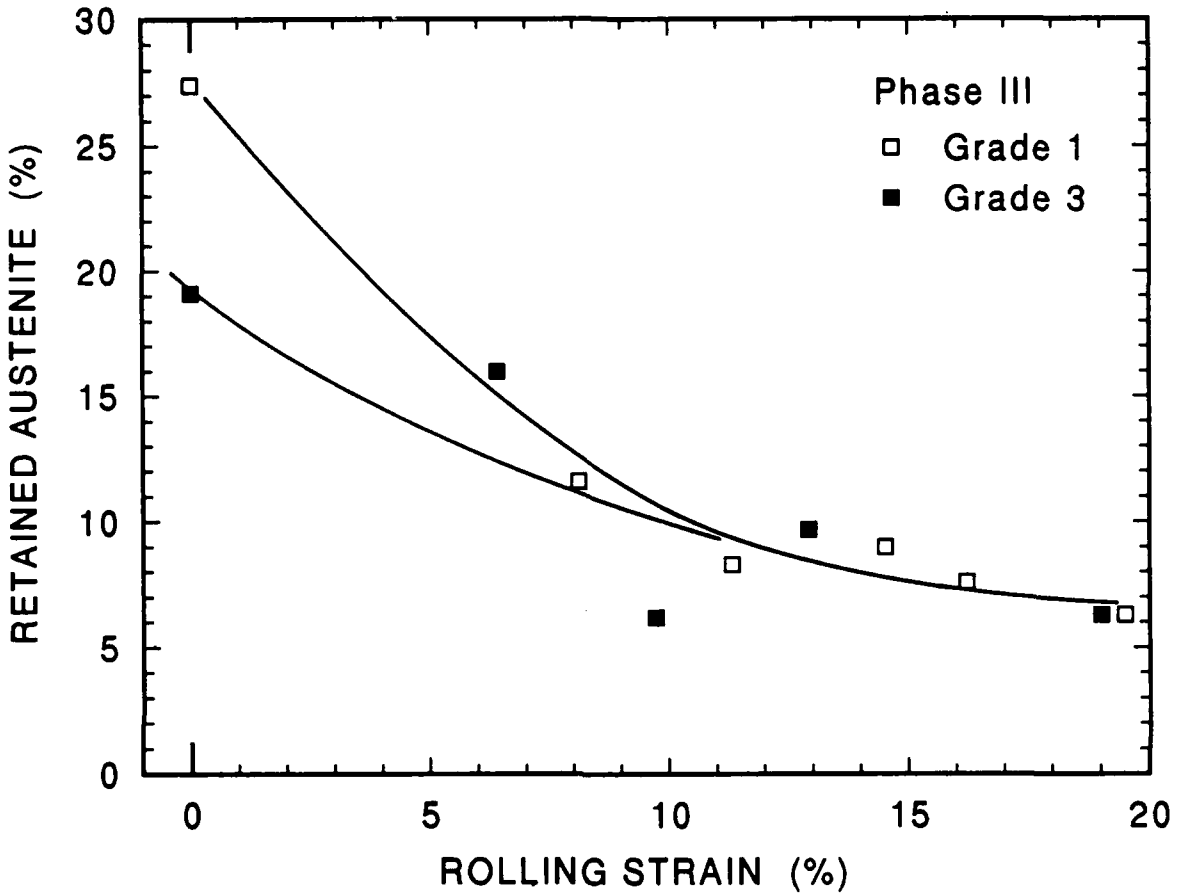

Figure 14: The effect of rolling strain on the retained austenite volume fraction from Phase III, Grade 1 and Grade 3 samples.

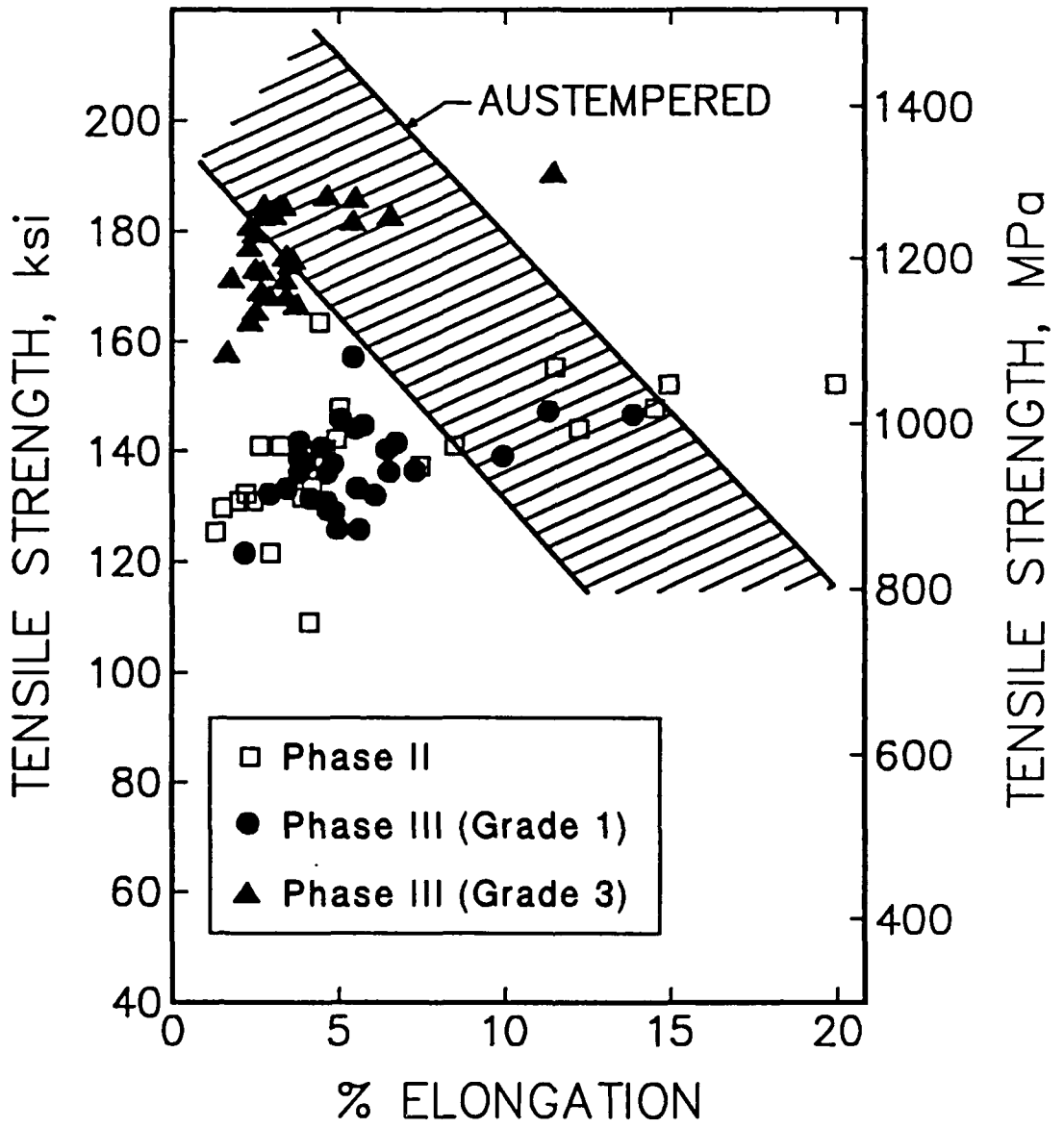

Figure 15: Summary of ultimate tensile strengths and ductilities for all of the Phase II and Phase III tensile samples. Also shown are the results, in the highlighted band, from a series of ductile irons as reported in the literature (1).

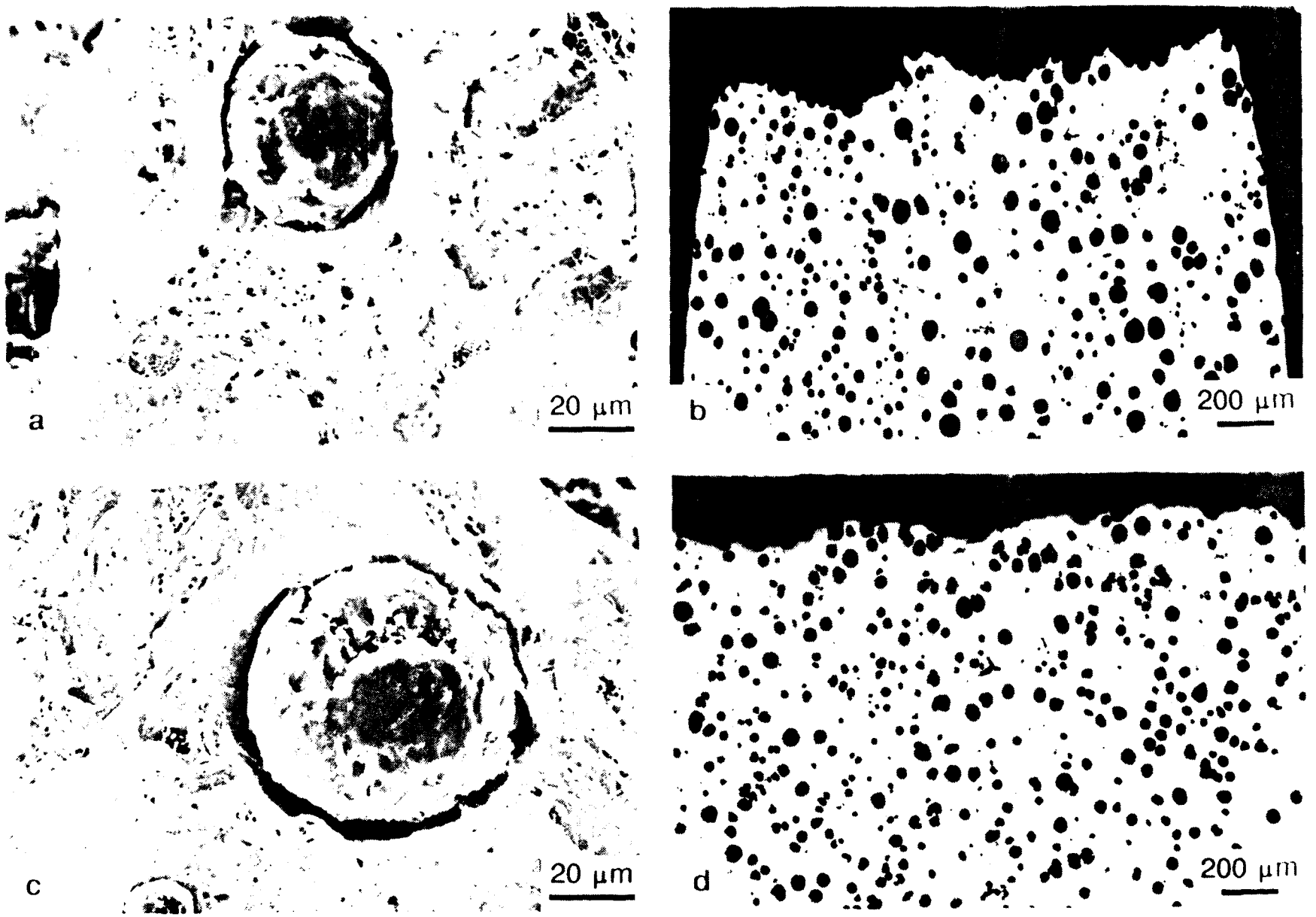

Figure 16: Tensile fracture surfaces of selected samples from Phase II. (a) SEM photograph, sample ADI29, tested at 120°C. (b) Light micrograph of cross section of fracture surface of sample in Fig. 16a. (c) SEM photograph, sample ADI16, tested at -30°C. (d) Light micrograph of cross section of fracture surface of sample in Fig. 16c.

DISTRIBUTION LIST

No. of Copies	To
1	Office of the Under Secretary of Defense for Research and Engineering, The Pentagon, Washington, D.C. 20301
	Director, U.S. Army Research Laboratory, 2800 Powder Mill Road, Adelphi, MD 20783-1197
1	ATTN: AMSRL-OP-SD-TP, Technical Publishing Branch
1	ATTN: AMSRL-OP-SD-TM, Records Management Administration
	Commander, Defense Technical Information Center, Cameron Station, Building 5, 5010 Duke Street, Alexandria, VA, 22304-6145
2	ATTN: DTIC-FDAC
1	MIAC/CINDAS, Purdue University, 2595 Yeagar Road, West Lafayette, IN, 47905
	Commander, Army Research Office, P.O. Box 12211, Research Triangle Park, NC 27709-2211
1	ATTN: Information Processing Office
	Commander, U.S. Army Materiel Command, 5001 Eisenhower Avenue, Alexandria, VA, 22333-0001
1	ATTN: AMCSCI
1	ATTN: AMCRD-M, Mr. Michael Baccellieri
	Commander, U.S. Army Missile Command, Redstone Scientific Information Center, Redstone Arsenal, AL 35898-5241
1	ATTN: AMSMI-RD-CS-R/Doc
	Commander, U.S. Army Armament, Munitions and Chemical Command, Dover, NJ 07801
1	ATTN: SMCAR-AET
	Commander, U.S. Army Armament Research Development and Engineering Center, Dover, NJ, 07806-5000
1	ATTN: AMSMC-PBR, Mr. William Donnelly
1	ATTN: AMSMC-PBR-M(D), Mr. Al Gonsiska
1	ATTN: AMSMC-PBR-M(D), Mr. Ferdinand del Carmen
1	ATTN: SMCAR-CCH-P, Mr. William Sharpe
	Director, U.S. Army Research Laboratory-Weapons Technology Directorate, Aberdeen Proving Ground, MD 21005
1	ATTN: AMSRL-OP-CI-B
	Director, Benét Weapons Laboratory, LCWSL, USA AMCCOM, Watervliet, NY 12189
1	ATTN: AMSMC-LCB-TL
	Director, Benét Weapons Laboratory, Watervliet, NY, 12189-4050
1	ATTN: SMCAR-CCB-TL
1	ATTN: SMCAR-CCB-SM, Mr. Alex Wakulenko
1	ATTN: SMCAR-CCB-SE, Mr. Peter Thorton
1	ATTN: SMCAR-CCB-RM, Dr. Paul Cote
1	ATTN: SMCAR-CCB-RM, Mr. Edward Troiano
	Commander, U.S. Army Tank-Automotive Command, Warren, MI 48397-5000
1	ATTN: AMSTA-TSL, Technical Library
1	ATTN: AMSTA-TMF, Mr. James W. Ogilvy
1	ATTN: AMSTA-UDM, Mr. Michael Trautman
1	ATTN: AMSTA-RTS, Mr. Bobby J. Wright
1	ATTN: AMSTA-TFP, Mr. Jeffery S. Parks
1	ATTN: AMSTA-RTT, Mr. Robert Smith
1	ATTN: AMSTA-RTT, Mr. Geza Szakacs
	Commander, Rock Island Arsenal, Rock Island, IL, 61299
1	ATTN: SMCRI-SEM-A, Ms. Cynthia Krist
1	ATTN: SMCRI-SEM-T, Mr. Richard Kalkan
1	ATTN: SMCRI-SEM-T, Mr. Cesar Cardenas
	Commander, U.S. Army Foreign Science and Technology Center, 220 7th Street, N.E., Charlottesville, VA 22901-5396
1	ATTN: AIFRTC, Applied Technologies Branch, Gerald Schlesinger
	Naval Research Laboratory, Washington, D.C. 20375
1	ATTN: Code 5830
	Naval Sea System Command, Washington, DC, 20326-5101
1	ATTN: Code 03R5, Mr. John Williams
	Naval Surface Warfare Center, Dahlgren, VA, 22448-5000
1	ATTN: Code G32, Mr. O.J. Huey
	Commander, U. S. Air Force Wright Research & Development Center, 2977 P Street STE6, Wright Patterson Air Force Base, OH, 45433-6523
1	ATTN: WL/MT-Bldg 653, Dr. Siamack Mazdiyasni

DISTRIBUTION LIST

No. of Copies	To
	Ductile Iron Society, North Olmstead, OH, 44070,
1	ATTN: Mr. Jack Hall
	Wagner Castings Company, P.O. Box 1319, Decatur, Il, 62525
1	ATTN: Dr. P.H. Mani
	Lufkin Industries, P.O. Box 849, 300 Winston Street, Lufkin, TX, 75902-0849
1	ATTN: Mr. Fred L. Preston
	Applied Process, Inc.,12238 Newburgh Road, Livonia, MI, 48150
1	ATTN: Mr. John Keough
	Colorado School of Mines, Dept. of Metallurgical and Materials Engineering, Golden, CO, 80401
1	ATTN: Prof. David Matlock
1	ATTN: Prof. George Krauss
	Michigan Technological University, Dept. of Metallurgy and Materials Engineering, 1400 Townsend Drive, Houghton, MI, 49931-1295
1	ATTN: Prof. Karl Rundman
	Northwestern University, Department of Materials Science and Engineering, Steel Research Group, Evanston, IL, 60208
1	ATTN: Prof. Gregory B. Olson
	Director, US Army Research Laboratory, Watertown, MA, 02172-0001
2	ATTN: AMSRL-OP-WT-IS, Technical Library
1	ATTN: AMSRL-OP-WT-IS, Visual Information
1	ATTN: AMSRL-OP-PR-WT
5	ATTN: AMSRL-MA-CC, Dr. Martin G.H. Wells, COR